

Imaging of ependymomas: MRI and CT

E. L. Yuh · A. J. Barkovich · N. Gupta

Received: 10 March 2009 / Published online: 10 April 2009

© The Author(s) 2009. This article is published with open access at Springerlink.com

Abstract The imaging features of intracranial and spinal ependymoma are reviewed with an emphasis on conventional magnetic resonance imaging (MRI), perfusion MRI and proton magnetic resonance spectroscopy, and computed tomography. Imaging manifestations of leptomeningeal dissemination of disease are described. Finally, salient imaging features obtained in the postoperative period to evaluate completeness of surgical resection, and thereafter for long-term surveillance for disease recurrence, are reviewed.

Keywords Ependymoma · MRI · CT · MR perfusion · Spinal ependymoma

Introduction

Magnetic resonance imaging (MRI) is the primary imaging modality used for the assessment of both intracranial and spinal ependymoma. Although computed tomography (CT) provides better demonstration of small or subtle calcifications within tumors, MRI provides superior delineation of the extent of tumor due to its greater soft tissue contrast, multiplanar imaging capability, and ability to obtain complementary information with T1- and T2-weighted

sequences. Finally, MRI avoids the use of ionizing radiation, a desirable strategy in children who are more susceptible to radiation-induced malignancy than adults [5].

The standard MRI protocol for pediatric intracranial tumors at UCSF includes volumetric fluid-attenuated inversion recovery (FLAIR), sagittal and axial T1-, axial T2-, axial diffusion-, and postcontrast axial and coronal T1-weighted sequences. In suspected infratentorial tumors, postcontrast sagittal T1-weighted images are also obtained. Susceptibility-weighted perfusion MRI and proton magnetic resonance (MR) spectroscopy are performed in a limited number of cases, usually to distinguish posttreatment changes from recurrent tumor in the posttherapeutic setting, or occasionally when the neoplastic nature of a primary lesion is in question. MRI of pediatric spinal tumors generally consists of sagittal T1-, T2-, and postgadolinium T1-weighted sequences, with axial T2- and postgadolinium T1-weighted images through the lesion.

Magnetic resonance imaging and computed tomography of intracranial tumors

General

Intracranial ependymomas, including both infra- and supratentorial ependymomas, generally demonstrate low T1, high T2, and intermediate-to-high FLAIR signal intensity relative to both gray and white matter (Figs. 1, 2, and 3). These characteristics have been attributed to the high proportion of ependymomas with intracellular myxoid accumulation and cyst formation [9]. As a result, they are often conspicuous on T2-weighted and FLAIR sequences and are also usually visible on unenhanced T1-weighted images (Figs. 1 and 2).

E. L. Yuh · A. J. Barkovich
Neuroradiology Section, Department of Radiology,
University of California, San Francisco (UCSF),
San Francisco, USA

N. Gupta (✉)
Departments of Neurological Surgery and Pediatrics,
University of California, San Francisco (UCSF),
San Francisco, USA
e-mail: guptan@neurosurg.ucsf.edu

Fig. 1 Classic MRI appearance of posterior fossa ependymoma in a 2-year-old child. Fourth ventricular mass demonstrates **a** low T1 signal intensity, **b** predominantly solid enhancement on postgadolinium T1-weighted images, and **c** heterogeneous T2 hyperintensity. **d** Sagittal postgadolinium T1-weighted image demonstrates extension inferior through the foramen of Magendie onto the posterior aspect of the upper cervical cord, a feature that is highly suggestive of ependymoma



Although ependymomas are generally T1 hypointense and T2 hyperintense relative to brain parenchyma, both T1 and T2 signal intensity are heterogeneous within the tumor. This is particularly true for supratentorial ependymomas, which have a greater propensity than their infratentorial counterparts for extensive cyst formation [2] (Fig. 3). This may be attributable to their later clinical presentation and larger size at the time of discovery. Cystic areas of a lesion may follow fluid signal intensity on both T2-weighted and FLAIR sequences or may remain hyperintense on FLAIR due to proteinaceous fluid contents. Calcifications, which are common in both supratentorial and infratentorial ependymomas (approximately 50%), and old hemorrhage are generally very low in signal intensity on all MRI sequences.

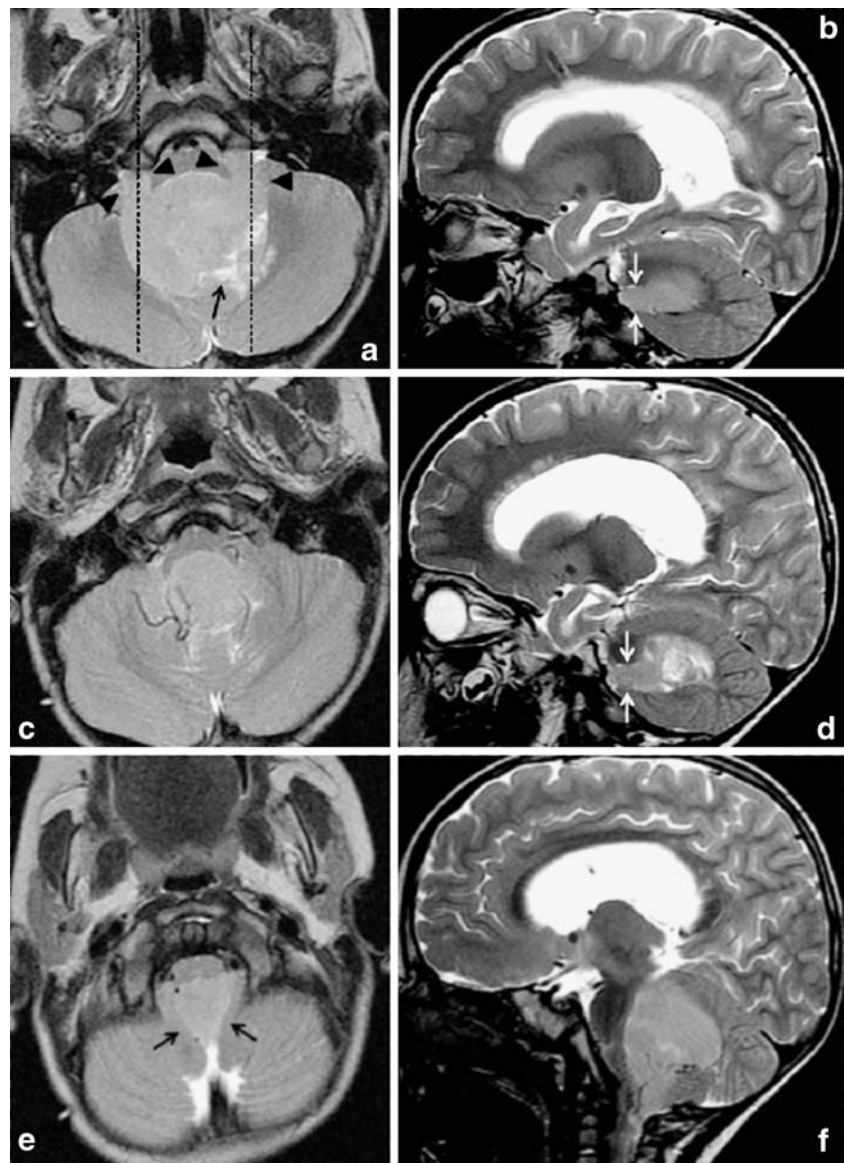
On postgadolinium T1-weighted images, there is usually avid enhancement of the soft tissue components of the tumor, intermixed with poorly enhancing or nonenhancing areas. A minority of lesions demonstrates little or no postgadolinium enhancement despite being composed of mostly soft tissue (Fig. 4).

Diffusion-weighted imaging (DWI) is based on the random movement of water molecules in tissue. Tissues in

which water diffusion is reduced demonstrate high DWI signal and low apparent diffusion coefficient (ADC). DWI demonstrates reduced diffusion within the soft tissue components of some ependymomas (Fig. 5), presumably due to high cellularity of some lesions. Diffusivity of ependymomas is generally intermediate between that of pilocytic astrocytomas and primitive neuroectodermal tumors [18]. However, diffusivity values are not completely reliable in making histologic diagnoses.

Perfusion MRI and proton MR spectroscopy are performed in only a limited number of cases, usually to distinguish treatment changes from recurrent tumor, or occasionally when the neoplastic nature of a lesion is in question. Perfusion MRI can be performed using several techniques, including T2*-weighted dynamic susceptibility and fast spoiled gradient-echo techniques, which require bolus administration of gadolinium contrast, and arterial spin labeling, which does not require gadolinium. Perfusion MRI is challenging in infants and young children for several reasons including the difficulty of obtaining proximal intravenous access, the use of small intravenous catheters that limit injection rates, the necessity of using

Fig. 2 Axial and sagittal T2-weighted images through a typical fourth ventricle ependymoma demonstrate signal intensity similar to gray matter throughout most of the lesion. Extension through the foramina of Luschka is demonstrated by *black arrowheads* in **a** and *white arrows* in **b** and **d**, and extension through foramen of Magendie by *black arrows* in **e**. *Dashed lines* in **a** indicate planes at which sagittal images (**b**, **d**) are located. The lesion insinuates around and encases vessels, as shown in **c** and **f**. Cystic/necrotic areas (*black arrows* in **a** and **d**) are closer to cerebrospinal fluid signal intensity

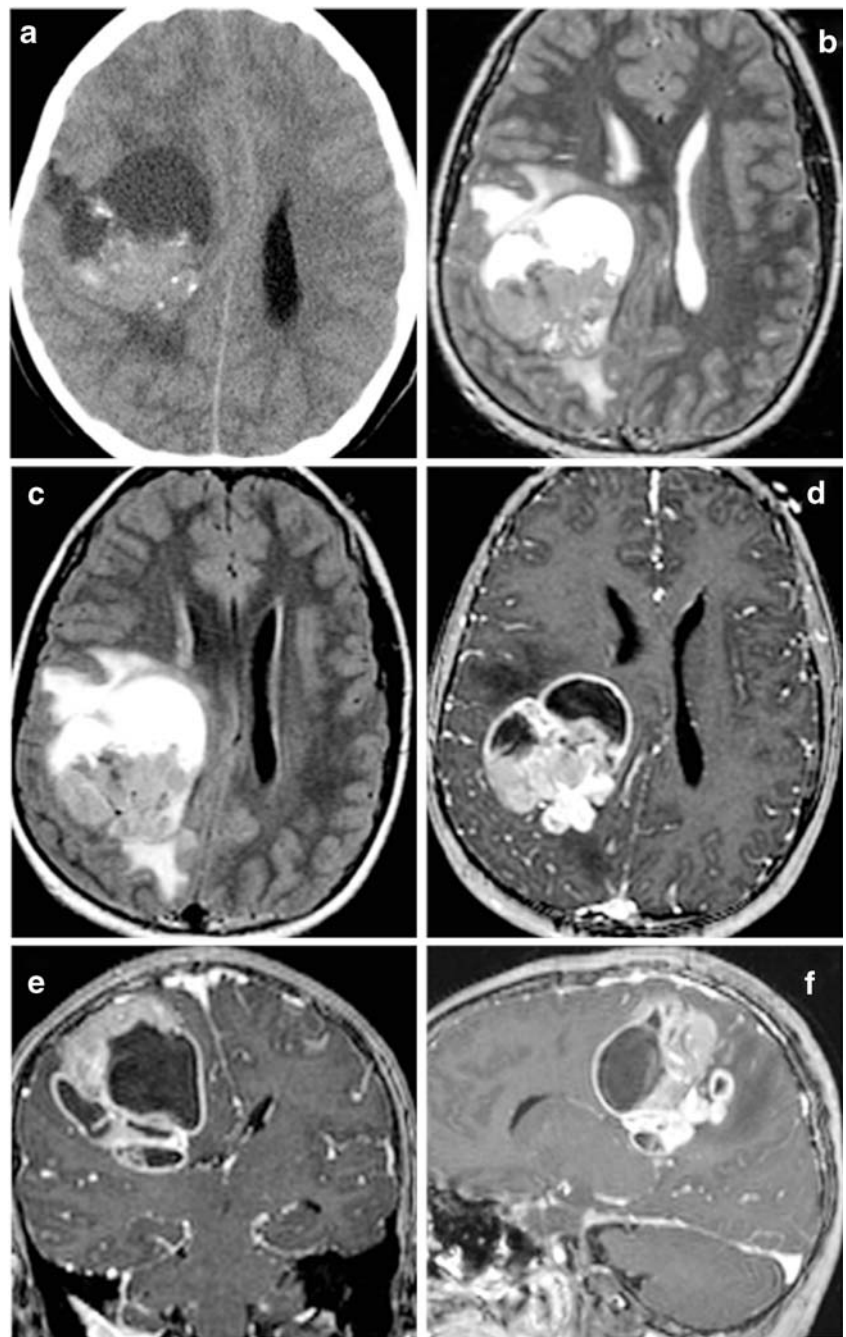


small doses of contrast, and high incidence of motion artifact [3]. When performed, perfusion MRI of ependymoma generally demonstrates markedly elevated cerebral blood volume and, unlike many other glial neoplasms, poor return to baseline that may be attributable to fenestrated blood vessels and an incomplete blood–brain barrier [22] (Figs. 5 and 6).

Proton MR spectroscopy usually demonstrates elevated choline and reduced N-acetylaspartate (NAA) in ependymomas, as in many other brain tumors. Although the use of MR spectroscopy for prospective differentiation of infratentorial ependymoma from medulloblastoma has been investigated, the variability in choline/NAA ratios within each tumor histology results in considerable overlap, and MR spectroscopy is currently used primarily to differentiate tumor recurrence from postradiation or posttreatment change rather than to confirm a histologic diagnosis [3].

MRI is the recommended initial brain imaging modality of choice not only for intracranial tumors but also for any younger child with new neurological signs or symptoms, except in the setting of acute head trauma [3]. However, intracranial ependymoma is sometimes initially diagnosed on head CT. CT demonstrates isodense or mildly hyperdense soft tissue portions of the tumor, calcifications in 50% of lesions, hemorrhage in approximately 10% [21], and often heterogeneous enhancement (Figs. 3a and 5, inset). CT is generally more sensitive for, and will demonstrate a greater number of, calcifications than most MRI sequences, particularly spin echo-type sequences. However, MRI sequences with increased susceptibility-associated signal loss, such as diffusion-weighted and gradient-echo sequences, commonly demonstrate foci of signal void/loss in areas of coarse/gross calcification or hemorrhage (Figs. 3 and 5).

Fig. 3 Supratentorial ependymoma in a 10-year-old girl on **a** noncontrast CT, **b** T2-weighted, **c** FLAIR, and **d–f** postgadolinium T1-weighted MRI. Unlike posterior fossa ependymomas, most supratentorial ependymomas (70%) are extraventricular in origin. Supratentorial ependymomas usually demonstrate more heterogeneous T1 and T2 signal than their infratentorial counterparts, due to a greater tendency toward cyst formation, calcifications, and hemorrhage. Avidly enhancing areas are generally present, but are often intermixed with poorly or nonenhancing areas

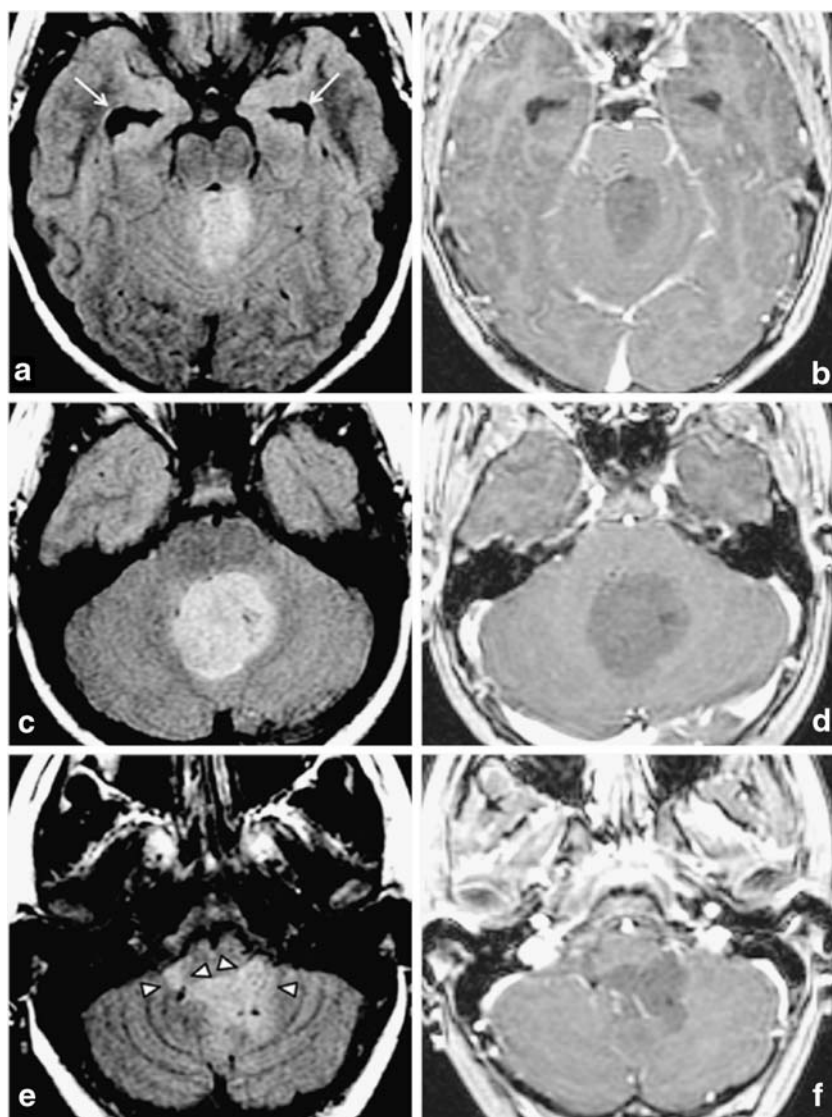


Infratentorial ependymoma

Approximately 70% of intracranial ependymomas are infratentorial, arising from differentiated ependymal cells lining the fourth ventricle and foramina of Luschka. At the time of clinical presentation, infratentorial ependymomas usually fill and distend the fourth ventricle, resulting in hydrocephalus and symptoms of nausea and vomiting in 90% of patients [1, 3]. A highly typical feature of ependymoma is extension through the foramina of Luschka into the cerebellopontine angle (15%) and/or inferiorly through the foramen of Magendie (60%) onto the posterior aspect of the upper

cervical cord (Figs. 1, 2, and 4). Although this feature is not entirely pathognomonic, the few medulloblastomas (the main differential diagnosis for infratentorial ependymoma) that extend through the fourth ventricular exit foramina [4] show more bulbous extension rather than thin tongues of tissue through the foramina as in ependymomas [3]. Ependymomas often insinuate around and within structures, encasing vessels and lower cranial nerves, and can cause cranial neuropathies. In addition to the classic appearance of a fourth ventricular mass, infratentorial ependymomas can also present within the cerebellopontine angle, presumably arising from the rests of ependymal cells therein. Ependymomas

Fig. 4 Atypical, nonenhancing ependymoma in a 13-year-old. **a, c, e** Homogeneous FLAIR hyperintensity throughout most of the lesion, which insinuates around and encases vessels and extends through the foramina of Luschka (*arrowheads* in **e**). Temporal horn dilatation (*arrows* in **a**) indicates hydrocephalus. As shown on postgadolinium T1-weighted images in **b, d, and f**, this lesion, unlike most ependymomas, demonstrates no appreciable enhancement, remaining diffusely hypointense on postgadolinium T1-weighted images



arising from a location not in the midline may have a worse prognosis than midline lesions, perhaps due to involvement of critical structures such as cranial nerves [3, 12].

Supratentorial ependymoma

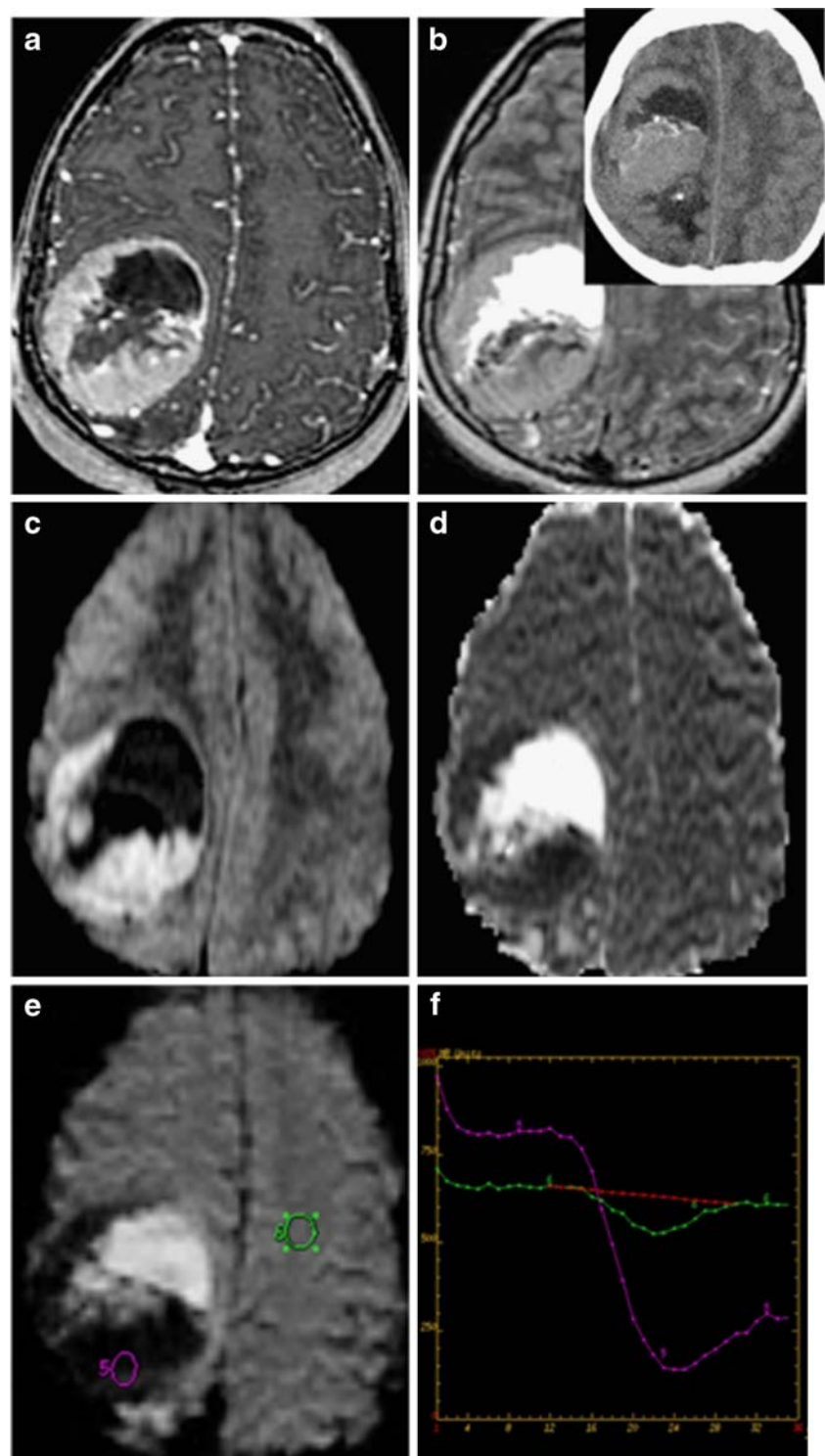
Approximately 30% of intracranial ependymomas are supratentorial. Within the pediatric population, supratentorial ependymomas are often seen in older childhood [11]. Unlike posterior fossa ependymomas, most supratentorial ependymomas (70%) are extraventricular in origin, arising within the brain parenchyma of the cerebral hemispheres rather than from ependymal cells lining the ventricular surfaces. Extraventricular ependymomas are thought to originate from the rests of ependymal cells that are retained in the brain parenchyma during embryonic development. They are, however, often located near the ventricular margins and may extend into the ventricular system. In addition, in

comparison to posterior fossa tumors, hydrocephalus occurs relatively late (after development of significant subfalcine herniation), by which time the tumors are typically large, with an average size of over 4 cm at presentation (Figs. 3, 5, and 6) [2, 9]. Approximately 30% of supratentorial ependymomas arise in an intraventricular location, generally along the surfaces of the lateral ventricles or along the septum pellucidum. Although the ependymal surface area of the third ventricle is larger than that of the fourth ventricle, third ventricular ependymomas are rare [10, 13].

Anaplastic ependymoma

The World Health Organization classifies ependymal tumors into four types: (1) ependymoma (grade 2), (2) anaplastic ependymoma (grade 3), (3) subependymoma (grade 1), and (4) myxopapillary ependymoma (grade 1). Grade 2 ependymomas are further subdivided into four

Fig. 5 Supratentorial ependymoma on **a** postgadolinium T1; **b** FLAIR (*inset*: noncontrast CT); **c** diffusion-weighted images (DWI); **d** apparent diffusion coefficient; and **e** perfusion MRI with **f** cerebral blood volume measurements. DWI demonstrates reduced diffusion within the soft tissue components of some ependymomas due to high cellularity. Perfusion-weighted imaging generally demonstrates elevated blood volume within the tumor, with poor return to baseline likely attributable to lack of a blood–brain barrier. CT demonstrates isodensity or mild hyperdensity of solid soft tissue portions of the tumor, often heterogeneous enhancement on postcontrast CT (not shown) and calcifications in 50% of lesions. Although CT is more sensitive for calcification than most MRI sequences, susceptibility-sensitive diffusion- and perfusion-weighted sequences in **c** and **e**, as well as gradient-echo sequences, do commonly demonstrate areas of calcification or hemorrhage as signal void/loss

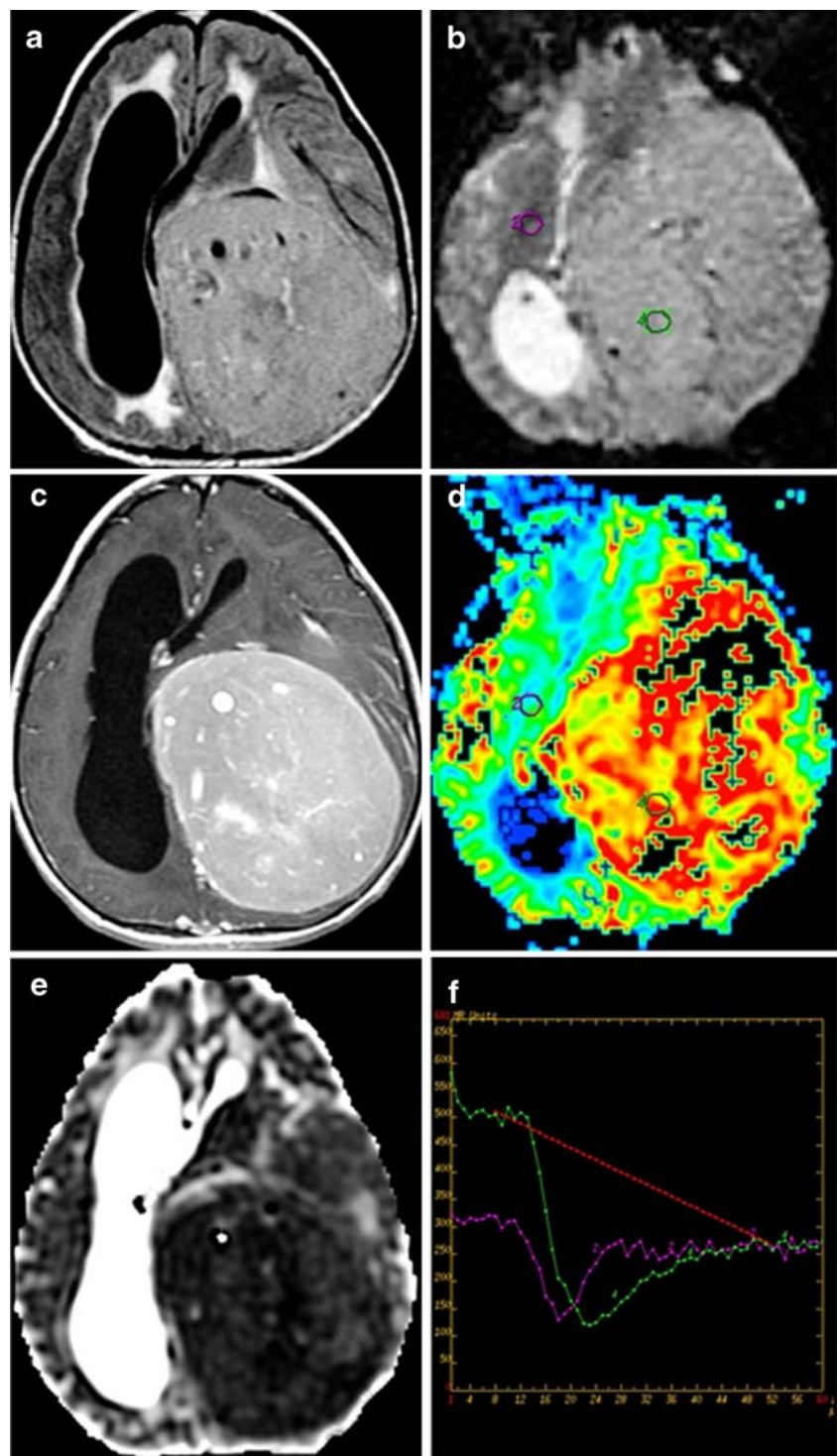


major histologic subtypes: cellular, papillary, clear-cell, and the rare tancytic subtype, with these subtypes demonstrating some variation in prognosis [10, 16]. In comparison to the more common grade 2 ependymomas, anaplastic ependymomas have greater incidence of cerebrospinal fluid dissemination at the time of diagnosis and a poorer prognosis (Fig. 7) [3].

Spinal ependymoma

Ependymoma is the second most common pediatric intramedullary spinal tumor after astrocytoma. Ependymomas constitute 30% of pediatric intramedullary spinal lesions, while astrocytomas constitute 60%. Most pediatric spinal ependymomas are WHO grade 2 lesions. Myxopapillary

Fig. 6 Supratentorial grade 2 ependymoma in a 12-year-old girl. **a** Axial FLAIR, **b** axial perfusion MRI, **c** postcontrast axial T1, **d** axial cerebral blood volume map derived from perfusion MRI, **e** axial ADC coefficient, and **f** perfusion MRI T2*-weighted dynamic susceptibility curves

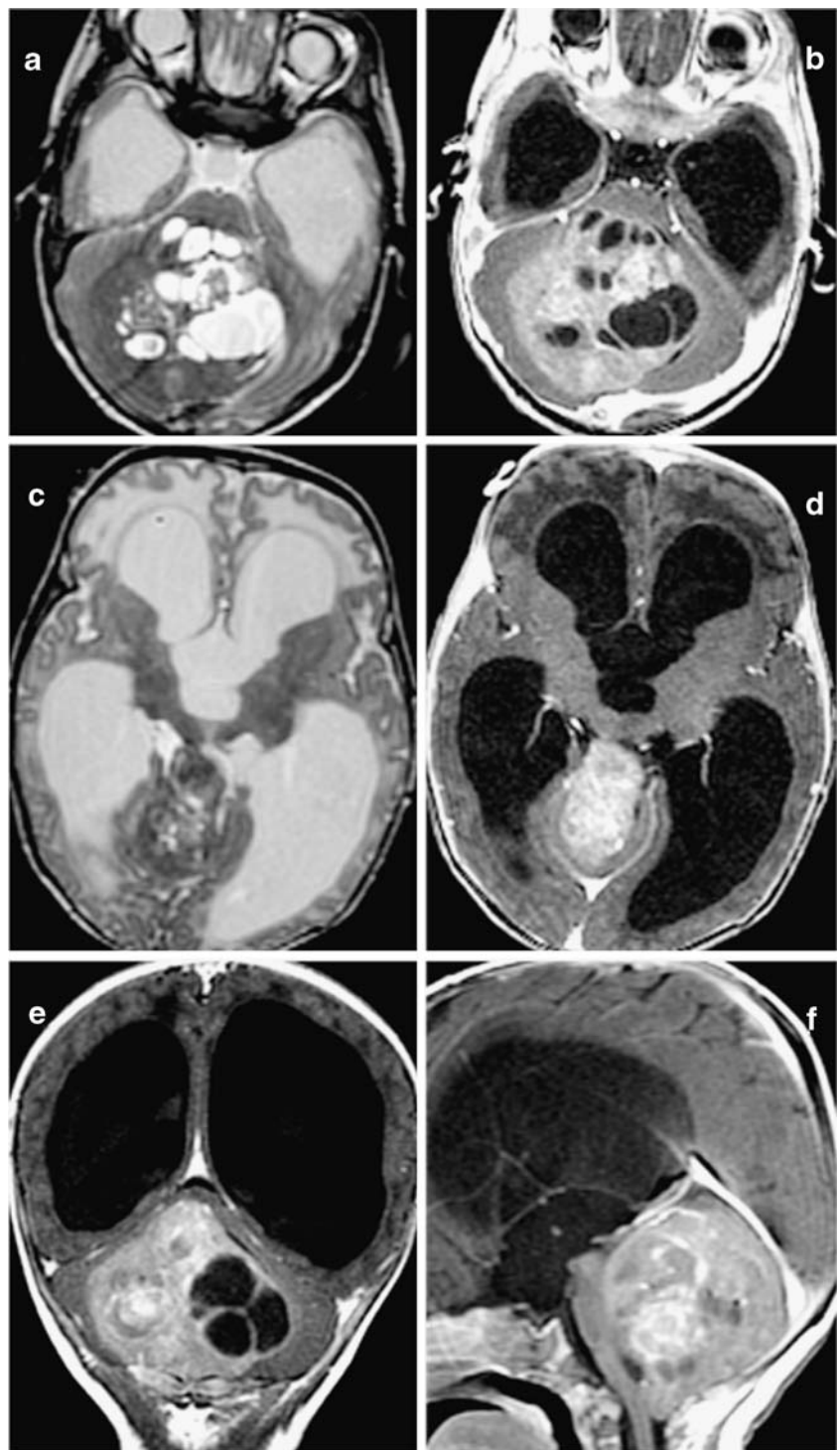


ependymoma, a WHO grade 1 lesion that occurs almost exclusively within the conus or cauda equina, is more common in adults, accounting for nearly 50% of adult spinal ependymomas, but is rare in children, comprising only 8% to 12% of pediatric spinal ependymomas [3]. As with their intracranial counterparts, prognosis in pediatric

spinal ependymoma is most dependent on tumor grade, completeness of resection, and evidence of disseminated disease at time of diagnosis.

As with their intracranial counterparts and most other intramedullary tumors, spinal ependymomas generally demonstrate high T2 and low T1 signal intensity that is

Fig. 7 Anaplastic ependymoma in a 2-month-old infant who presented with increasing head circumference. T2-weighted sequences in **a** and **c** and postgadolinium T1-weighted sequences in **b**, **d**, **e**, and **f**. This tumor is characterized by multiple cysts, heterogeneous postcontrast enhancement, and large size resulting in severe obstructive hydrocephalus. **c**, **d** Upward extension of the tumor through the tentorial incisura



often heterogeneous (Fig. 8). Contrast enhancement may be homogeneous or heterogeneous, but some enhancement is nearly always present. Ependymomas have a greater tendency than astrocytomas to be located centrally in the cord, and often demonstrate a sharper margin of enhancement, corresponding to margins of the tumor, than do astrocytomas [3]. Although seen in only 20% of cases, a finding of T2 hypointensity along the borders of the lesion,

attributable to remote episodes of hemorrhage, is highly suggestive of ependymoma [3]. As with their intracranial counterparts, cerebrospinal fluid (CSF) dissemination at the time of diagnosis is rare but is somewhat more common with higher-grade tumors. Perfusion MRI and MR spectroscopy are not currently performed on spinal tumors due to the small axial cross-section of the spinal canal and susceptibility effects from the surrounding bony spine [3].

Fig. 8 Typical spinal ependymomas. **a–c** T2-, T1-, and postgadolinium T1-weighted sagittal images of grade 2 ependymoma in a 3-year-old boy. **d–f** T2-, T1-, and postgadolinium T1-weighted images of a myxopapillary (grade 1) ependymoma in a 14-year-old boy

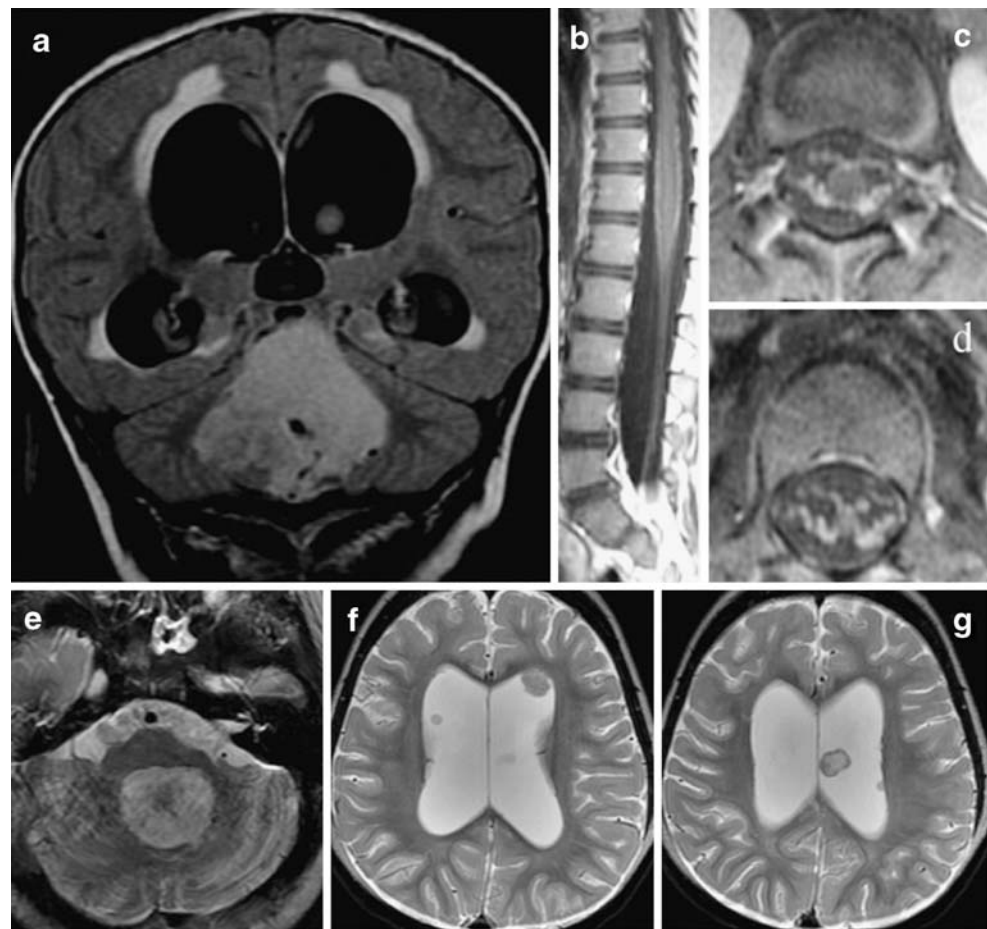


Leptomeningeal dissemination

Evidence of spread of ependymoma cells into the CSF is a key factor in staging, prognosis, and treatment [15]. Subarachnoid spread of disease can be detected by MRI (Fig. 9) or by CSF cytologic studies. MRI is more sensitive than, and has replaced, CT myelography in the detection of leptomeningeal spread [7] and is also likely more sensitive than CSF cytology for the detection of subarachnoid spread of primary brain tumors (though CSF cytology may be more sensitive for CSF spread of leukemias and lymphomas) [3, 6].

Despite their location close to the ependymal surfaces of the ventricles and central canal of the spinal cord that could be expected to lead to a high incidence of exfoliation into the subarachnoid space, subarachnoid seeding is relatively uncommon in comparison to other primary central nervous system neoplasms such as medulloblastomas and malignant astrocytomas [15]. In general, CSF seeding is more common in higher-grade ependymomas, such as anaplastic ependymomas, and in younger children [15, 17, 19]. CSF spread is also much more common with infratentorial tumors than with supra-

Fig. 9 Leptomeningeal and multiple intraventricular metastases discovered 13 months after treatment of a posterior fossa ependymoma in a 2-year-old girl. Although initial MRI of the lumbar spine was suggestive of possible leptomeningeal disease, CSF cytology was negative. **a)** Original coronal FLAIR images at time of diagnosis. **b)** Sagittal and **c), d)** axial postgadolinium T1-weighted images of the lumbar spine at time of diagnosis. **e)** Thirteen months later, the resection site of the original fourth ventricular tumor demonstrates no evidence of locally recurrent disease. **f)** However, multiple intraventricular leptomeningeal metastases are seen and may have been attributable to CSF spread at the time of initial diagnosis



tentorial tumors [14]. A study of 754 patients with intracranial ependymomas demonstrated cytologic evidence of CSF spread of disease in 12%, with a lower incidence (<5%) of symptomatic leptomeningeal disease [19]. Another study showed positive CSF cytology in only 8% of a series of 26 grade 2 intracranial ependymomas and 33% of 15 grade 3 anaplastic ependymomas and grade 2/3 ependymomas with anaplastic features [15]. Detectable subarachnoid spread of disease at the time of presentation of grade 2 ependymoma is also much less common than in medulloblastoma. Rather, when subarachnoid spread does occur, it is often detected at the time of discovery of disease recurrence. The mean time from diagnosis to discovery of CSF dissemination is 6.8 years [3, 17].

Imaging manifestations of leptomeningeal spread of disease in the spine are variable and include smooth enhancement along the surface of the spinal cord; enhancing foci in the extramedullary intradural or, occasionally, intramedullary space; nerve root thickening, nodularity, or clumping; and thecal sac irregularity. The lumbosacral region, particularly the most caudal aspect of the thecal sac, is the most common location for “drop” metastases. MR sensitivity

for leptomeningeal metastases increases with higher doses of contrast and the use of volumetric gradient-echo imaging to obtain thin section axial imaging of the spine. Small metastases on nerve roots can be detected if thin sections (3 mm or less) are used. Of note, if MRI for assessment of subarachnoid tumor spread is performed postoperatively, it should be performed no less than 2 weeks following surgery, as “leakage” of contrast into the subarachnoid and subdural space following posterior fossa craniectomy can occur and mimic leptomeningeal spread of disease [3, 23, 24].

Intracranial imaging manifestations include leptomeningeal nodules, masses or smooth enhancement, and communicating hydrocephalus. Interestingly, intraventricular nodules and masses often demonstrate little or no enhancement (Fig. 9) [3].

Postoperative imaging

As with other intracranial neoplasms, an MRI is obtained immediately after surgery to evaluate the extent of resection and periodically thereafter for long-term surveillance for disease recurrence. Following surgery, a thin rim of enhance-

ment (likely representing granulation tissue) can be seen along the cavity margins beginning as soon as 24 h, which becomes progressively thicker and more nodular over the next several days. Therefore, imaging to assess extent of resection should be performed less than 48 h after surgery [3]. Pregadolinium T1-weighted sequences are always included to distinguish perioperative hemorrhage from residual enhancing tumor. For pediatric patients, a head CT in the immediate postoperative period after craniotomy is reserved for delayed recovery from anesthesia or unexpected acute neurologic deficits or to assess changes in hydrocephalus after shunt placement [3]. It should not be used as a surrogate for MR imaging to assess extent of resection.

Following the period after surgery, enhancement along the resection cavity margins progressively decreases beginning at approximately 5 weeks and usually resolves completely within 12 months [3]. Therefore, any new or increasing enhancement after approximately 5 weeks after surgery should raise suspicion for tumor recurrence. New contrast enhancement can also be seen several months to years (typically 4 to 6 months) after radiation therapy and has been attributed to late delayed injury resulting from permanent damage to blood vessels [3]. Since recrudescence enhancement is sometimes attributable to these posttreatment effects rather than recurrent tumor, proton MR spectroscopy and perfusion MRI can be helpful adjunct techniques in this setting to aid in the differentiation of tumor recurrence from posttreatment changes. In particular, necrosis, including that due to radiation injury, generally demonstrates concomitant reduction of NAA, choline, and creatine peaks, while a new or persistently elevated choline/NAA ratio raises concern for recurrent tumor.

Although recommendations regarding the duration of surveillance imaging vary [8, 20, 24], periods of up to 10 years have been suggested for posterior fossa ependymoma. Because a complete resection is not feasible in many patients due to insinuation of the tumor around vessels, cranial nerves, and other critical structures, ependymomas do show a relatively high recurrence rate [3, 8, 11, 20, 24].

Open Access This article is distributed under the terms of the Creative Commons Attribution Noncommercial License which permits any noncommercial use, distribution, and reproduction in any medium, provided the original author(s) and source are credited.

References

- Allen JC, Siffert J, Hukin J (1998) Clinical manifestations of childhood ependymoma: a multitude of syndromes. *Pediatr Neurosurg* 28:49–55
- Armington WG, Osborn AG, Cubberley DA, Harnsberger HR, Boyer R, Naidich TP, Sherry RG (1985) Supratentorial ependymoma: CT appearance. *Radiology* 157:367–372
- Barkovich AJ (2005) *Pediatric neuroimaging*. Lippincott, Williams and Wilkins, London
- Blaser SI, Harwood-Nash DC (1996) Neuroimaging of pediatric posterior fossa medulloblastoma. *J Neurooncol* 29:23–34
- Brody AS, Frush DP, Huda W, Brent RL (2007) Radiation risk to children from computed tomography. *Pediatrics* 120:677–682
- Freilich RJ, Krol G, DeAngelis LM (1995) Neuroimaging and cerebrospinal fluid cytology in the diagnosis of leptomeningeal metastasis. *Ann Neurol* 38:51–57
- Koeller KK, Sandberg GD (2002) From the archives of the AFIP. Cerebral intraventricular neoplasms: radiologic–pathologic correlation. *Radiographics* 22:1473–1505
- Kramer ED, Rafto S, Packer RJ, Zimmerman RA (1991) Comparison of myelography with CT follow-up versus gadolinium MRI for subarachnoid metastatic disease in children. *Neurology* 41:46–50
- Lefton DR, Pinto RS, Martin SW (1998) MRI features of intracranial and spinal ependymomas. *Pediatr Neurosurg* 28:97–105
- Maksoud YA, Han YS, Engelhard HH (2002) Intracranial ependymomas. *Neurosurg Focus* 13(3):1–5
- Mermuys K, Jeuris W, Vanhoenacker PK, Van Hoe L, D'Haenens P (2005) Best cases from the AFIP: supratentorial ependymoma. *Radiographics* 25:486–490
- Nagib MG, O'Fallon MT (1996) Posterior fossa lateral ependymoma in childhood. *Pediatr Neurosurg* 24:299–305
- Oppenheim JS, Strauss RC, Mormino J, Sachdev VP, Rothman AS (1994) Ependymomas of the third ventricle. *Neurosurgery* 34:350–352, discussion 352–353
- Packer RJ, Siegel KR, Sutton LN, Litmann P, Bruce DA, Schut L (1985) Leptomeningeal dissemination of primary central nervous system tumors of childhood. *Ann Neurol* 18:217–221
- Qian X, Goumnerova LC, De Girolami U, Cibas ES (2008) Cerebrospinal fluid cytology in patients with ependymoma: a bi-institutional retrospective study. *Cancer* 114:307–314
- Ragel BT, Townsend JJ, Arthur AS, Couldwell WT (2005) Intraventricular tanyctic ependymoma: case report and review of the literature. *J Neurooncol* 71:189–193
- Rezai AR, Woo HH, Lee M, Cohen H, Zagzag D, Epstein FJ (1996) Disseminated ependymomas of the central nervous system. *J Neurosurg* 85:618–624
- Rumboldt Z, Camacho DL, Lake D, Welsh CT, Castillo M (2006) Apparent diffusion coefficients for differentiation of cerebellar tumors in children. *AJNR Am J Neuroradiol* 27:1362–1369
- Salazar OM (1983) A better understanding of CNS seeding and a brighter outlook for postoperatively irradiated patients with ependymomas. *Int J Radiat Oncol Biol Phys* 9:1231–1234
- Steinbok P, Hentschel S, Cochrane DD, Kestle JR (1996) Value of postoperative surveillance imaging in the management of children with some common brain tumors. *J Neurosurg* 84:726–732
- Swartz JD, Zimmerman RA, Bilaniuk LT (1982) Computed tomography of intracranial ependymomas. *Radiology* 143:97–101
- Uematsu Y, Hirano A, Llena JF (1988) Electron microscopic observations of blood vessels in ependymoma. *Neurol Surg* 16:1235–1242
- Wiener MD, Boyko OB, Friedman HS, Hockenberger B, Oakes WJ (1990) False-positive spinal MR findings for subarachnoid spread of primary CNS tumor in postoperative pediatric patients. *AJNR Am J Neuroradiol* 11:1100–1103
- Wootton-Gorges SL, Foreman NK, Albano EA, Dertina DM, Nein PK, Shukert B, Cesario KB, Gage S, Rumack CM, Strain JD (2000) Pattern of recurrence in children with midline posterior fossa malignant neoplasms. *Pediatr Radiol* 30:90–93